# 2D Flow Past a Confined Circular Cylinder with Sinusoidal Ridges

Kieran Cavanagh[1*]
Dr. Rachmadian Wulandana[2]
[1,2]Mechanical Engineering Program, State University of New York at New Paltz, New Paltz, NY, USA. [*]Dept. of Mathematics, State University of New York at New Paltz

## 1. Introduction

Flow past a circular cylinder is a classical problem in fluid mechanics. Cylindrical structures immersed in viscous flow, such as smokestacks, bridge struts, measurement instruments, medical devices, etc., are common in engineering applications, so understanding the flow physics in these situations is of prime importance. While a significant amount of work has been done analyzing viscous flow past an unconfined circular cylinder, there is significantly less work studying the same problem with a confined cylinder. These situations arise in applications such as pipe flow, blood flow through arteries, or in situations where the scaling of a particular experiment requires wall effects to be taken into consideration. There are various effects imposed on the flow in the confined case, particularly when the cylinder is confined to a plane channel. For example, when no-slip conditions on the walls are assumed, the velocity profile becomes parabolic as opposed to uniform. The von Kármán vortex street that appears at the onset of the laminar periodic shedding regime exhibits different behavior when confined to a plane channel, as the walls limit the motion of vortices moving perpendicular to the flow [1]. Furthermore, a variety of effects have been noted when the ratio of cylinder diameter to channel width (also known as blocking ratio) changes. For instance, evidence suggests that the critical Reynolds number marking the start of the periodic shedding regime increases with increasing blocking ratio [2]. This is likely because the walls inhibit the oscillation of the near-wake tail, hence enhancing the stability of the near-wake region and postponing the transition to the periodic shedding regime [3].

Surface roughness can have a considerable effect on the flow physics, as well, most notably at high Reynolds numbers. While most surface roughness has a relatively random pattern, predictable forms of roughness can appear in certain contexts. For example, consistent waviness resembling sinusoidal waves can appear on the surface of 3D printed solids (see Figure 1) due to vibrations caused by the 3D printing process or external events. The effect of surface roughness is primarily studied at high Reynolds numbers [4], but in the present study we study the flow effects at Reynolds numbers in the steady laminar and periodic shedding regimes.

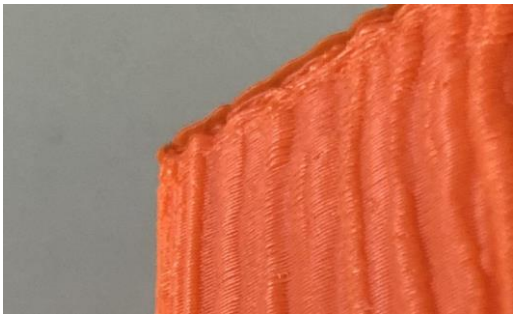

**Figure 1**: Waviness on 3D printed solid

We use the CFD Module of COMSOL Multiphysics 5.4 to simulate two-dimensional flow past a circular cylinder with consistent sinusoidal ridges confined to a plane channel with fixed blocking ratio. Flow effects are studied at Reynolds numbers of 20, 50, 200, and 500. We perform steady and time-dependent simulations to measure a variety of quantities of interest, such as the recirculation zone length and drag coefficient in the laminar regime (corresponding to Re = 20 and 50), and the Strouhal number, peak-to-peak lift coefficient amplitude, and mean drag coefficient in the periodic shedding regime (corresponding to Re = 200 and 500).

## 2. Problem Formulation

To model the sinusoidal ridges, we parametrically define the cylinder boundary in polar coordinates by

$$r(\theta) = \frac{L}{2} + a \cdot \cos(\omega\theta), \quad 0 \le \theta \le 2\pi$$

Where L is the base cylinder diameter, $a$ is the amplitude of the ridges, and $\omega$ is the total number of ridges. For all simulations, we select $L = 0.15$m. Motivated by the size of the observation chamber utilized in a closed loop water flow tank available in Mechanical Engineering Program of our campus, the two-dimensional computational domain is selected to have channel length and width of $20L$ and $3L$, respectively. Following Schäfer[5], the center of the cylinder is positioned in the center of the channel, a

distance $2L$ from the inlet. An inlet velocity with a parabolic profile is chosen at the leftmost wall, and a zero-pressure outlet boundary condition is chosen at the rightmost wall. The inlet velocity is ramped up from zero in order to ensure the solver can find consistent initial values. Physics-controlled mesh, calibrated for laminar flow, is generated by COMSOL, with the element size set to Finer. The domain with mesh is shown in Figure 2.

**Figure 2.** Computational domain with mesh

We define the Reynolds number based on the base cylinder diameter $L$ and the centerline (maximum) velocity $U_c$:

$$Re = \frac{\rho U_c L}{\mu}$$

Additionally, we define the Strouhal number $St$, and drag and lift coefficients, $C_D$ and $C_L$, using the well-known formulation:

$$St = \frac{fL}{U_c},\ C_D = \frac{2F_D}{\rho U_c L},\ C_L = \frac{2F_L}{\rho U_c L}$$

Where $f$ is the frequency of vortex shedding, which is equivalent to the frequency of the time-dependent lift coefficient oscillation, and $F_D$ and $F_L$ are the total drag and lift forces acting on the cylinder, respectively.

## 3. Equations and Numerical Methods

In this study, for cases involving time-dependency, corresponding to Re = 200 and Re = 500, COMSOL solves the velocity fields $\boldsymbol{u}$ using the time-dependent Navier-Stokes equations for incompressible laminar flow:

$$\rho \frac{\partial \boldsymbol{u}}{\partial t} + \rho\,(\boldsymbol{u}\cdot\nabla)\boldsymbol{u} = \nabla\cdot[-p\boldsymbol{I} + \boldsymbol{K}] + \boldsymbol{F}$$

Here, the first and second terms on the left hand side represent the unsteadiness and convective acceleration, respectively. On the right hand side, the fluid forces due to hydrostatic pressure and fluid shear stresses are included on the first term. In particular, for incompressible fluid, the stress tensor is presented simply as a linear relationship

$$\boldsymbol{K} = \mu(\nabla\boldsymbol{u} + (\nabla\boldsymbol{u})^T)$$

where $\mu$ is the fluid viscosity. Lastly, the vector $\boldsymbol{F}$ is the volume force vector. The above differential equations are solved along with the incompressibility restriction;

$$\rho\,\nabla\cdot(\boldsymbol{u}) = 0$$

In the stationary cases of this study, corresponding to Re = 20 and Re = 50, the unsteady term is ignored from the equation and the $\boldsymbol{u}$ does not depend on time.

To compute the drag and lift, COMSOL integrates the stresses along the cylinder wall in the $x$ and $y$ directions, respectively. Other statistics related to the time-dependent lift and drag coefficients, such as the mean $C_D$, the Strouhal number, and the peak-to-peak $C_L$ amplitude, are computed using a custom script written in MATLAB. The script determines the simulation time associated with the steady state of vortex shedding (see Figure 3), and then processes the lift and drag coefficient data after that point.

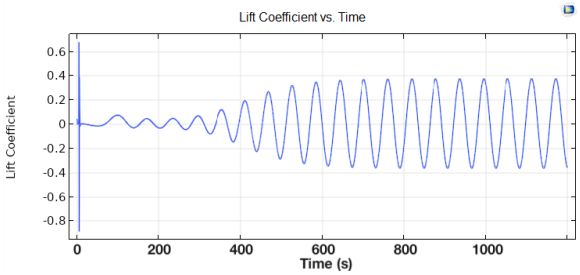


**Figure 3.** Example lift coefficient versus time plot for Re = 200. After $t = 650$s, $C_L(t)$ has a consistent amplitude.

For all time-dependent simulations, we use a perturbation in the form of short-lived vertical (y-direction) oscillation of the cylinder, where the wall moves at the following equation-driven velocity:

$$v(t) = \frac{U_c}{10} R(t-4)\sin\big(15(t-4)\big)\,e^{-2(t-4)}$$

Where $R(t)$ is an appropriate ramp function to ensure the solver can find consistent initial values. The constants used are chosen mostly arbitrarily, with the exception of the amplitude $U_c/10$ (chosen as such so the perturbation is significantly smaller than the inlet velocity) and the time shift of 4 seconds (so the perturbation is triggered a few seconds into the simulation). Figure 4 shows a plot of the perturbation as a function of time. It should be noted that the perturbation only impacts the transient phase - after performing simulations to verify this, we concluded that the perturbation has no effect on the steady state solution.

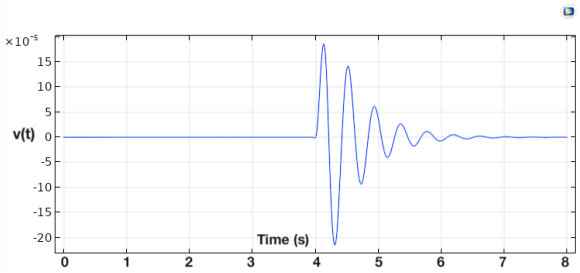


**Figure 4.** Perturbation velocity versus time

In the stationary case, in order to compute the length of the recirculation zone $l_r$, which is another variable of interest (see figure 5), MATLAB is used to find the stagnation point behind the cylinder, which corresponds to finding the point of minimum velocity along the horizontal domain centerline.

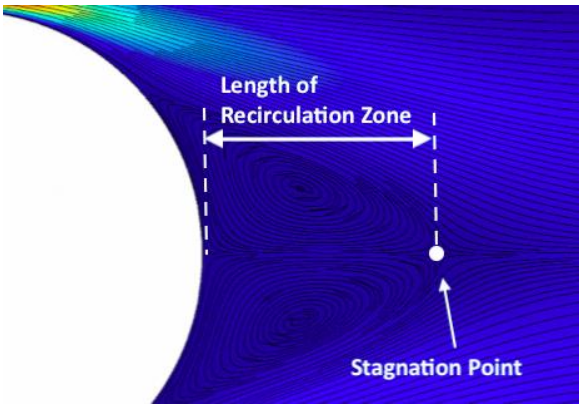


**Figure 5.** Stagnation point and length of recirculation zone

## 4. Verification

In order to verify the correctness of the selected computational method, applied inlet perturbation, mesh density, as well as the custom numerical code in MATLAB, we attempt to replicate the results of established studies in the literature, namely, of flow past a *smooth* circular cylinder.

Shafer (1996) collected benchmark computations of flow past a circular cylinder confined to a plane channel with similar blocking ratio and Reynolds numbers as we study [5]. To verify our methods for the stationary case, we simulate the two-dimensional steady case (2D-1) studied by Shafer. We use a similar mesh (Physics-controlled, Finer element size) and the same computational methods described above to compute key quantities of interest above. In particular, we compute the length of the recirculation zone $l_r$, drag coefficient $C_D$, and lift coefficient $C_L$. Our results match closely, although our values tend to be slightly smaller than Shafer. Table 1 summarizes the results, along with the upper and lower bounds of possible "exact" values given by Shafer [5].

**Table 1.** Summary of stationary verification study

| | $l_r$ | $C_D$ | $C_L$ |
|---|---|---|---|
| Present study | 5.56 | 0.00958 | 0.0770 |
| Shafer lower bound | 5.57 | 0.0104 | 0.0842 |
| Shafer upper bound | 5.59 | 0.0110 | 0.0852 |

To verify our methods for the time-dependent case, we perform simulations similar to those of Singha and Sinhamahapatra (2010)[6]. In particular, we use their geometric setup at a blocking ratio of 3 (using their definition) and a Reynolds number of 200, and apply our mesh and computational methods to determine $C_{D,mean}$, $C_{L,rms}$, and $St$. Our results are in excellent agreement with Singha and Sinhamahapatra's, with the exception of a slight discrepancy in the $C_{L,rms}$ values. Table 2 summarizes these results.

**Table 2.** Summary of time-dependent verification study

| | $C_{D,mean}$ | $C_{L,rms}$ | $St$ |
|---|---|---|---|
| Present study | 1.421 | 0.263 | 0.233 |
| Sinha and Sinhamahapatra[6] | 1.423 | 0.272 | 0.233 |

## 5. Results and Discussion

### 5.1 Stationary Results

In the stationary case, we performed simulations to test the effect of changing the number of ridges $\omega$ on the length of the recirculation zone $l_r$ and the drag coefficient $C_D$. Ultimately, we found that the length of the recirculation zone is independent of the number of ridges. For both $Re = 20$ and $Re = 50$, the recirculation zone length is the same as that of a smooth cylinder for $\omega$ from 5 to 25. This confirms the idea that $l_r$ should primarily depend on the blocking ratio and Reynolds number. However, for $\omega = 4$, $l_r$ is slightly less than the others, which is indicative of the fact that $\omega = 4$ corresponds to a qualitatively different geometry than that of a cylinder.

We found an increasing relationship between $C_D$ and $\omega$ for Re = 20 and Re = 50, which can be seen in figures 6 and 7. For both Reynolds numbers, $C_D$ is higher when $a$ is larger $(L/25)$, which may be due to the greater channel blocking

effect. Additionally, $C_D$ as a function of $\omega$ gets closer to $C_D$ for a smooth cylinder as $\omega$ increases, although it is still lower. This may be evidence for the hypothesis that high numbers of ridges can roughly approximate a smooth cylinder, at least at low Reynolds numbers. It does not appear that this is the case in the turbulent flow regime, but that is beyond the scope of this paper [4]. Furthermore, the case of $\omega = 4$ does not fit with the main trend of the data in any case, which again points to the unique geometric nature of this case.

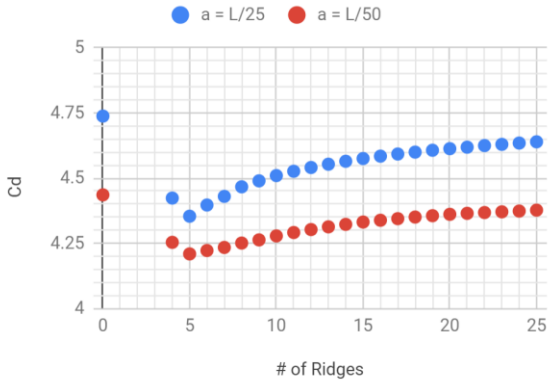


**Figure 6.** $C_D$ vs. $\omega$, $Re = 20$.

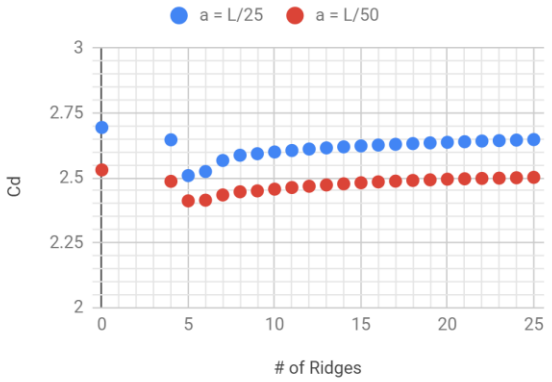


**Figure 7.** $C_D$ vs. $\omega$, $Re = 50$.

Additionally, due to the unique behavior for $\omega = 4$, we studied the effect of changing the angle of attack $\alpha$ (measured counterclockwise) on the drag coefficient $C_D$. The plots can be seen in figures 8 and 9. As expected, when $\alpha$ sweeps from 0 to 90 degrees, the result is symmetric due to the symmetry of the problem. For both Re = 20 and Re = 50, $C_D$ is larger when a = L/25, which is partially due to the increased channel blocking. Additionally, when $\alpha = 45°$, the drag coefficient reaches a minimum, and the difference between $C_D$ for each value of $a$ is smaller. This effect is more pronounced in the Re = 50 case.

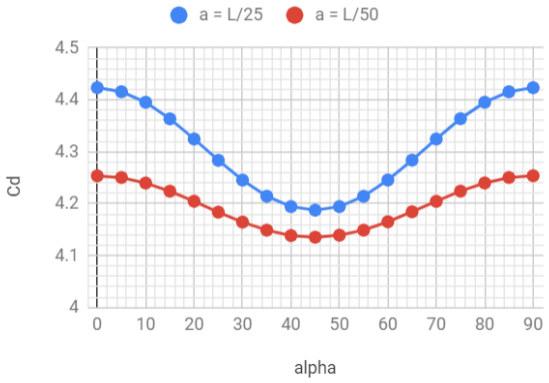


**Figure 8.** $C_D$ vs. $\alpha$, $Re = 20, \omega = 4$.

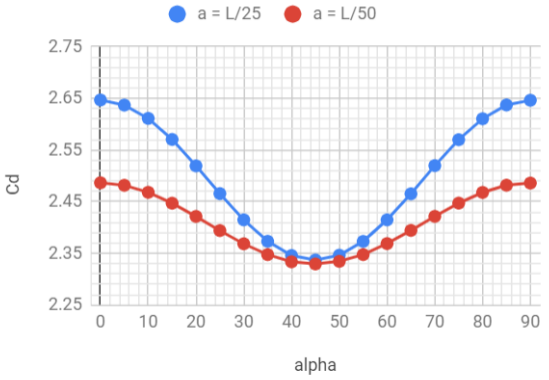


**Figure 9.** $C_D$ vs. $\alpha$, $Re = 50, \omega = 4$.

### 5.2 Time-Dependent Results

In the time-dependent case, we studied three quantities of interest: the Strouhal number St, the mean drag coefficient $C_{D,mean}$, and the peak-to-peak lift coefficient amplitude $C_{L,pkpk}$. Three parameters are varied: the ridge amplitude $a$, the number of ridges $\omega$, and the Reynolds number $Re$. In every plot that follows, we plot a quantity of interest versus the number of ridges. Parametric sweeps were performed for the case of zero ridges (corresponding to a smooth cylinder) and from 4 to 25 ridges. In one set of plots, we compare the effects of two different $Re$ values, while in the other set of plots, we compare the effects of two different values of $a$.

For the set of plots that compare values of $Re$, we keep $a = L/25$ fixed, and we compare the effects at $Re = 200$ and $Re = 500$. Figures 10, 11, and 12 show the effect of varying $Re$ on the $\omega$ −dependent progression of $St$, $C_{D,mean}$, and $C_{L,pkpk}$, respectively. A few key trends can be noted. First, as figure 10 shows, the Strouhal number tends to be higher when Re = 200. The same can be said for $C_{D,mean}$. The reverse is true for $C_{L,pkpk}$: for Re = 500, $C_{L,pkpk}$ tends to be higher.

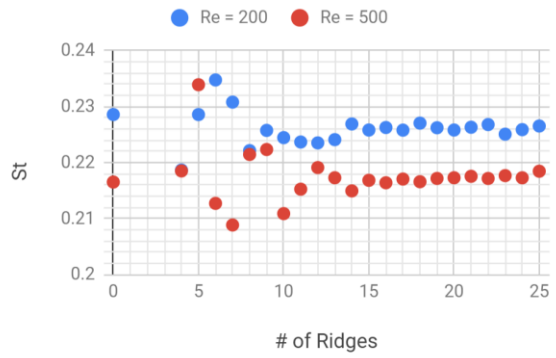


**Figure 10.** St vs. $\omega$, $Re = 200$ and 500 ($a = L/25$).

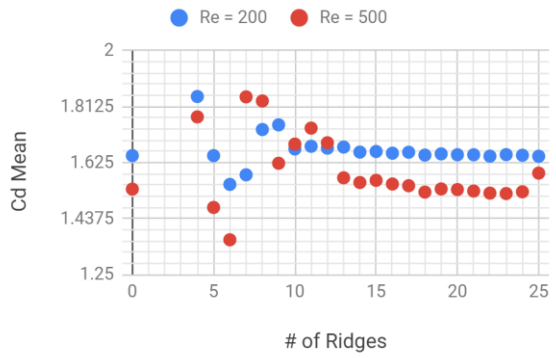


**Figure 11.** $C_{Dmean}$ vs. $\omega$, $Re = 200$ and 500 ($a = L/25$).

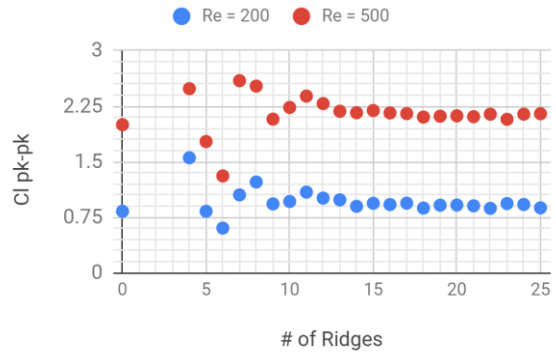


**Figure 12.** $C_{L,pkpk}$ vs. $\omega$, $Re = 200$ and 500 ($a = L/25$).

For the set of plots that compare values of $a$, we keep $Re = 500$ fixed, and we compare the effects of $a = L/50$ and $a = L/25$. Figures 13, 14, and 15 show the effect of varying $a$ on the $\omega$ −dependent progression of $St$, $C_{D,mean}$, and $C_{L,pkpk}$, respectively. Notice that only odd numbers of $\omega$ are present here. The plots show a few key trends. First, the Strouhal number tends to be slightly higher when the ridge height is smaller, as figure 12 shows. However, a larger ridge height causes $C_{D,mean}$ and $C_{L,pkpk}$ to be larger, as shown in figures 14 and 15.

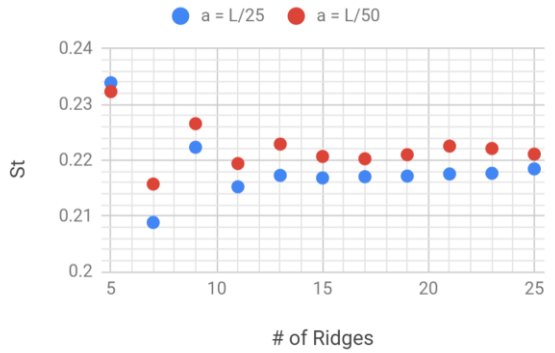


**Figure 13.** St vs. $\omega$, $a = L/25$ and $a = L/50$ ($Re = 500$).

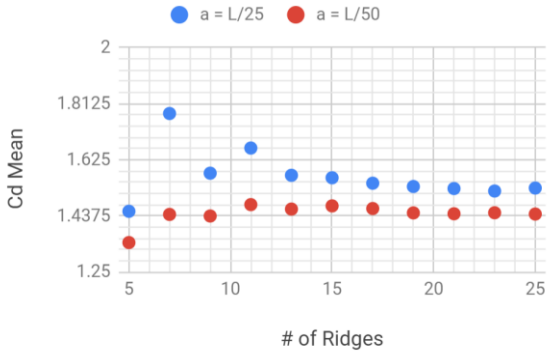


**Figure 14.** $C_{D,mean}$ vs. $\omega$, $a = L/25$ and $a = L/50$ ($Re = 500$).

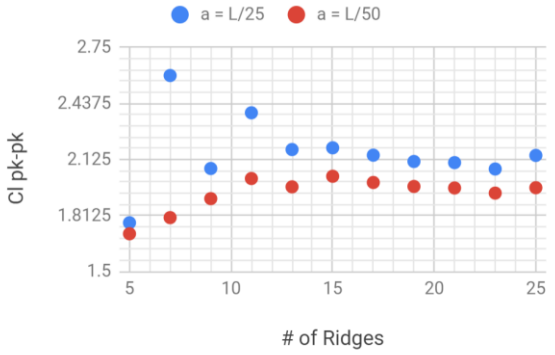


**Figure 15.** $C_{L,pkpk}$ vs. $\omega$, $a = L/25$ and $a = L/50$ ($Re = 500$).

There are also a few general trends that apply to all of the plots for the time-dependent case. First, for each plot, the results are very erratic and no clear trend can be deduced when $\omega$ is small, which is likely due to the qualitatively different geometry for small $\omega$. While there do tend to be clear trends in the stationary simulations (at lower Reynolds numbers) for $\omega$ between 5 and 13, it is likely that the higher Reynolds numbers of the present simulations accentuate the unique flow physics caused by the

qualitatively different geometry of the cylinders with $\omega$ in this range. Figures 10 and 11 show how the critical value of $\omega$ after which St and $C_{D,mean}$ as functions of $\omega$ become approximately steady tends to be higher when Re = 500, which supports the hypothesis that higher Re accentuates the effect of the different geometry at low $\omega$. For St, $C_{D,mean}$, and $C_{L,pkpk}$, the consistent values obtained after $\omega \approx 13$ closely approximate the value for the case of a smooth cylinder, which further supports the hypothesis that a cylinder with many ridges can, in some sense, approximate a smooth cylinder.

## 6. Conclusion and Further Research

Using the CFD module of COMSOL Multiphysics 5.4, we performed stationary and time-dependent simulations of flow past a confined circular cylinder with sinusoidal ridges, at a fixed blocking ratio. At four different Reynolds numbers, we varied the number of ridges and their amplitude and observed the effects.

In the stationary case, we determined that the length of the recirculation zone is independent of the number of ridges, while the drag coefficient generally increases as the number of ridges increases. Additionally, $C_D$ is larger when the ridge height is increased. We also studied the effect of changing the angle of attack for cylinder with four (4) ridges, and found that $C_D$ reaches a minimum when $\alpha = 45°$. This minimization is more pronounced for a larger ridge height.

In the time-dependent case, there is no clear relationship between any of the quantities studied and the number of ridges when $\omega < \sim 13$. However, after $\omega > \sim 13$, there tends to be little change in the value of most quantities. Most quantities as functions of $\omega$ tend to oscillate around this "steady" value before settling down to it. Additionally, we find that the mean drag coefficient and peak-to-peak lift coefficient are larger for a larger ridge height, but the opposite is the case for the Strouhal number.

There are also a few general observations about this particular cylinder geometry worth noting. First, a cylinder with four ridges has a qualitatively different geometry than other numbers of ridges. A similar effect can be seen for cylinders with less than ~13 ridges, as it is difficult to deduce clear trends for quantities measured in the time dependent case when $\omega < \sim 13$. Second, in some senses, a cylinder with a large number of ridges can approximate a smooth cylinder, although it is unclear whether this is due to decreased computational accuracy. Most quantities studied tended to approach the value for a smooth cylinder for high numbers of ridges. Finally, the results tentatively suggest that a higher Reynolds number accentuates the erratic behavior associated with the unique geometry of cylinders with relatively low numbers of ridges. This can be seen in the fact that $\omega = 4$ is the outlier in the stationary ($Re = 20$ and 50) tests, yet in the time dependent ($Re = 200$ and 500) tests, it is difficult to deduce a clear trend for any quantities when $\omega < \sim 13$.

As of now, little is understood about the precise flow physics past sinusoidally ridged circular cylinders. More research needs to be done to isolate the exact causes of the trends we have noted. Simulations and experiments in an unconfined domain would help eliminate the potential effect of blocking on the quantities studied here, and tests performed at a wider range of Reynolds numbers could help determine if there are discrepancies between Re-dependent relationships (such as $St$ as a function of $Re$) for smooth cylinders versus ridged cylinders. A cylinder with four ridges has a qualitatively different geometry as other ridged cylinders, so more tests would need to be performed to understand the unique flow physics in this situation.

## References


1. Zovatto, L. and Pedrizzetti, G., Flow about a circular cylinder between parallel walls, *Journal of Fluid Mechanics*, **440**, pp. 1-25 (2001)
2. Chen, J. H. et al., Bifurcation for flow past a cylinder between parallel planes, *Journal of Fluid Mechanics*, **284**, pp. 23-41 (1995)
3. Shair, F. H. et al., The effect of confining walls on the stability of the steady wake behind a circular cylinder, *Journal of Fluid Mechanics*, **17**, 546-50 (1963)
4. Zdravkovich, M. M., *Flow around circular cylinders: Volume II: Applications* (Vol. 2), pp. 748-798. Oxford University Press, New York, USA (2003)
5. Schäfer, M. et al., Benchmark computations of laminar flow around a cylinder, *Flow simulation with high-performance computers II*, pp. 547-566. Springer Vieweg Verlag, Germany (1996)
6. Singha, S. and Sinhamahapatra, K. P., Flow past a circular cylinder between parallel walls at low Reynolds numbers, *Ocean Engineering*, **37**, No. 8-9, pp. 757-769 (2010)


## Acknowledgements


1. SUNY New Paltz Summer Undergraduate Research Experience (SURE) Program for 2018
2. Seth Pearl (ME student) for pointing out the waviness on the 3D printed solids.